# Effects of aerosols and relative humidity on cumulus clouds

Jiwen Fan,[1] Renyi Zhang,[1] Guohui Li,[1] and Wei-Kuo Tao[2]

Received 11 October 2006; revised 17 April 2007; accepted 11 May 2007; published 24 July 2007.

[1] The influences of the aerosol type and concentration and relative humidity (RH) on cumulus clouds have been investigated using a two-dimensional spectral-bin cloud model. Three simulations are conducted to represent the polluted continental, clean continental, and marine aerosol types. Under the same initial dynamic and thermodynamic conditions, the maritime aerosol case results in more intensive radar reflectivity in both developing and mature stages than the continental aerosol cases, because of enhanced warm rain by collisions and ice processes by deposition growth due to larger droplet sizes and higher supersaturation, respectively. The considerable delay in convective development due to reduced droplet condensation is responsible for the longer cloud lifetime in the marine aerosol case. For the continental case, the most noticeable effects of increasing aerosol number concentrations (with 15 different initial values) are the increases of the cloud droplet number concentration and cloud water content but a decrease in the effective droplet radius. More latent heat release from increasing condensation results in stronger convection and more melting precipitation at the higher aerosol concentrations. Melting precipitation and secondary clouds primarily contribute to enhanced precipitation with increasing aerosols. The precipitation, however, decreases with increasing aerosol in the extremely high aerosol cases (over $5 \times 10^4$ cm$^{-3}$) due to suppression of convection from depleted water vapor and inefficient coalescence. When the initial aerosol concentration exceeds a critical level, most of the cloud properties become less sensitive to aerosols, implying that the aerosol effect on deep convection is more pronounced in relatively clean air than in heavily polluted air. The aerosol effect on the cloud properties is strongly dependent on RH. As the surface RH increases from 40 to 70%, the cloud changes from shallow warm to deep convective types due to a significant increase of convective available potential energy (CAPE). The aerosol effects on the cloud microphysical properties and precipitation are negligible in dry air (40% surface RH), but much more significant in humid air (60-70% surface RH). The rain delay is sensitive to RH, but not to aerosols under similar initial thermodynamic conditions.

**Citation:** Fan, J., R. Zhang, G. Li, and W.-K. Tao (2007), Effects of aerosols and relative humidity on cumulus clouds, *J. Geophys. Res.*, *112*, D14204, doi:10.1029/2006JD008136.

## 1. Introduction

[2] It is widely recognized that the aerosol-cloud interaction plays an important role in climate [e.g., *Penner et al.*, 2001; *Ramaswamy et al.*, 2001; *Zhang et al.*, 2004a]. The aerosol indirect effect refers to influence of aerosols on cloud microphysics, cloud duration, or precipitation [*Twomey*, 1977], and is considered to be one of the most uncertain elements in anthropogenic climate forcing [*IPCC*, 2001]. The impact of aerosols on cloud formation and development is highly uncertain in its magnitude. While there have been ample observations supporting the qualitative conclusions that aerosols reduce the cloud particle size for a fixed liquid water content [*Twomey*, 1977; *Liu et al.*, 2003], the aerosol effect on precipitation processes is even more uncertain, both in the magnitude and direction. It has been suggested that aerosols suppressed precipitations, as in the cases of smoke aerosols on tropical warm clouds, urban and industrial air pollution on stratocumulus and cumulus clouds, and desert dust on shallow convective clouds [e.g., *Rosenfeld*, 2000; *Rosenfeld and Woodley*, 2001]. On the other hand, precipitation enhancement was observed around heavily polluted coastal urban areas such as Houston [*Shepherd and Burian*, 2003] and Tokyo [*Ohashi and Kida*, 2002]. Field experiments and satellite data analyses showed that cloud droplet number concentration increased with aerosol number concentration in observed convection cases over land, while the effective radius appeared to be smaller in clouds over the land (polluted areas) than that over the ocean [e.g., *Ramanathan et al.*, 2001; *Heymsfield and McFarquhar*, 2001; *Liu et al.*, 2003]. *Andreae et al.* [2004] suggested

[1]Department of Atmospheric Sciences, Texas A&M University, College Station, Texas, USA.
[2]NASA Goddard Space Flight Center, Greenbelt, Maryland, USA.

Copyright 2007 by the American Geophysical Union.
0148-0227/07/2006JD008136

suppression of low-level rainout and aerosol washout which allows transport of water and smoke to upper levels, causing more intensive thunderstorms and release of more latent heat higher in the atmosphere. *Kaufman and Koren* [2006] recently reported an increase in cloud cover with increasing aerosol column concentrations. Elevated electrification and lightning activities in thunderstorms have been suggested to be associated with enhanced deep convection and mixed-phase processes linked to urban pollution [*Williams et al.*, 1991; *Orville et al.*, 2001], which may impact the air chemistry [*Nesbitt et al.*, 2000; *Bond et al.*, 2001; 2002; *Zhang et al.*, 2003]. In addition, polluted aerosols from the Asian continent have been linked to intensified storms over the Pacific [*Zhang et al.*, 2007].

[3] The aerosol effects on different cloud types have been studied with various numerical models in recent years. A pronounced increase in cloud droplet concentrations together with a substantial reduction of the effective droplet radius was found in polluted orographic clouds [*Maritinsson et al.*, 1999]. A high sensitivity of the rain rate and amount in cumulus clouds to the concentration and size of aerosols was identified in numerical simulations with spectral microphysics [*Reisin et al.*, 1996; *Khain et al.*, 1999; *Yin et al.*, 2000; *Khain et al.*, 2005]. The simulations using spectral-bin microphysical cloud models also revealed suppressed precipitation for deep convective clouds in a continental aerosol concentration [*Khain et al.*, 2004; *Khain and Pokrovsky*, 2004]. Using a 3-D large-eddy cloud model with a spectral microphysics, Feingold and co-workers found reduction in precipitation and complex responses of cloud properties with increasing aerosols for warm cumulus clouds [*Feingold et al.*, 2005; *Jiang and Feingold*, 2006; *Xue and Feingold*, 2006]. The work by *Jiang et al.* [2006] showed suppressed precipitation but an unchanged cloud lifetime for shallow cumulus with aerosol concentrations varying from clean to polluted conditions. Another recent numerical study investigated the responses of cloud physical processes of tropical deep convection to increasing aerosol/CCN concentrations using a 3-D cloud model with bulk microphysical schemes [*Wang*, 2005].

[4] Relative humidity is another key factor affecting cloud microphysics and dynamics. In air with different water vapor contents, the effects of aerosols on cloud developments and precipitation likely behave distinctly. *Khain et al.* [2005] performed and analyzed a set of experiments with different RH for continental and maritime conditions. It was shown that the magnitude of aerosol effects on precipitation and even its sign depend on RH. In the 3-D cloud simulations with spectral-bin microphysics by *Lynn et al.* [2005a, 2005b], the importance of the ambient RH on the precipitation was addressed.

[5] In this paper we present sensitivity studies of the aerosol type and concentration and relative humidity on cumulus clouds characteristic of the coastal city of Houston, Texas, using the cloud-resolving Goddard Cloud Ensemble (GCE) model with the spectral-bin microphysics described by *Khain et al.* [2004], in which melting is assumed at the freezing level, but with some additional modifications of the droplet nucleation procedure described by *Fan et al.* [2007]. The sensitivity of the cloud properties and precipitation to aerosols and RH are evaluated.

## 2. Description of Numerical Experiments and Data Analysis

[6] In a separate study, a convective cloud event occurring on August 24, 2000 in Houston, Texas was simulated using the spectral-bin microphysics and the results were compared to available measurements of radar reflectivity and precipitation [*Fan et al.*, 2007]. Our earlier simulation used realistic aerosol size distributions and compositions to represent the aerosol properties in this region. It was found that the chemical compositions of $(NH_4)_2SO_4$ and slightly soluble organics, with a reformulation of the Köhler theory to include the effect of slightly soluble organics and soluble gas of $HNO_3$ for aerosol activation, produced simulations better in agreement with the observations [*Fan et al.*, 2007]. The simulations well captured the major features observed in the convective cell, including the intensity, size, lifetime, and the accumulated rain.

[7] In the present work we report additional sensitivity studies to investigate the effects of aerosols and RH on cumulus clouds, with the above mentioned aerosol composition and activation scheme as the base run. The sounding used in the base run is from Houston, Texas with the longitude of 95.54W and latitude of 29.95N (Figure 1). The vertical temperature and dew point profiles reveal instability in the atmosphere, with a convective available potential energy (CAPE) of 960 J $kg^{-1}$ integrated from the surface. The surface temperature is about 31°C. The RH is about 60% at the surface and over 85% at about 1.5 km. The wind profiles from the sounding reveal weak wind shear. The computational domain is comprised of $1024 \times 33$ grid points with a horizontal resolution of 500 m. There are 33 stretched vertical levels with a resolution of 250 m at the lowest level and 1260 m at the top. Open boundary conditions are used at the lateral boundaries. More details of the initial thermodynamic and dynamic conditions and model configurations for the numerical experiments have been presented by *Fan et al.* [2007].

[8] We consider three cases to represent possible aerosol scenarios in the coastal city of Houston, Texas, dependent on the wind speed and directions [*Fan et al.*, 2005; *Li et al.*, 2005; *Fan et al.*, 2006; *Li et al.*, 2007]. The physical environment in this region includes frequent incursions of marine and continental air masses that receive emissions from woodlands and a major urban area containing large power plants and the largest concentrations of petrochemical refining activities in the world [*Lei et al.*, 2004; *Zhang et al.*, 2004b]. For example, a strong sea breeze in this region brings in large amounts of marine aerosols consisting of sea-salt from the Gulf of Mexico. In contrast, a strong northwest wind brings relatively clean continental air masses. We conduct three simulations to represent polluted continental (P-case), clean continental (C-case), and marine (M-case) aerosol types, on the basis of aerosol measurements and simulations in the Houston area [*Fan et al.*, 2005; *Fan et al.*, 2006]. The initial dynamic and thermodynamic conditions remain invariant for all three simulations in order to isolate the aerosol effects from the other factors. The P-case corresponds to the base run mentioned above, while

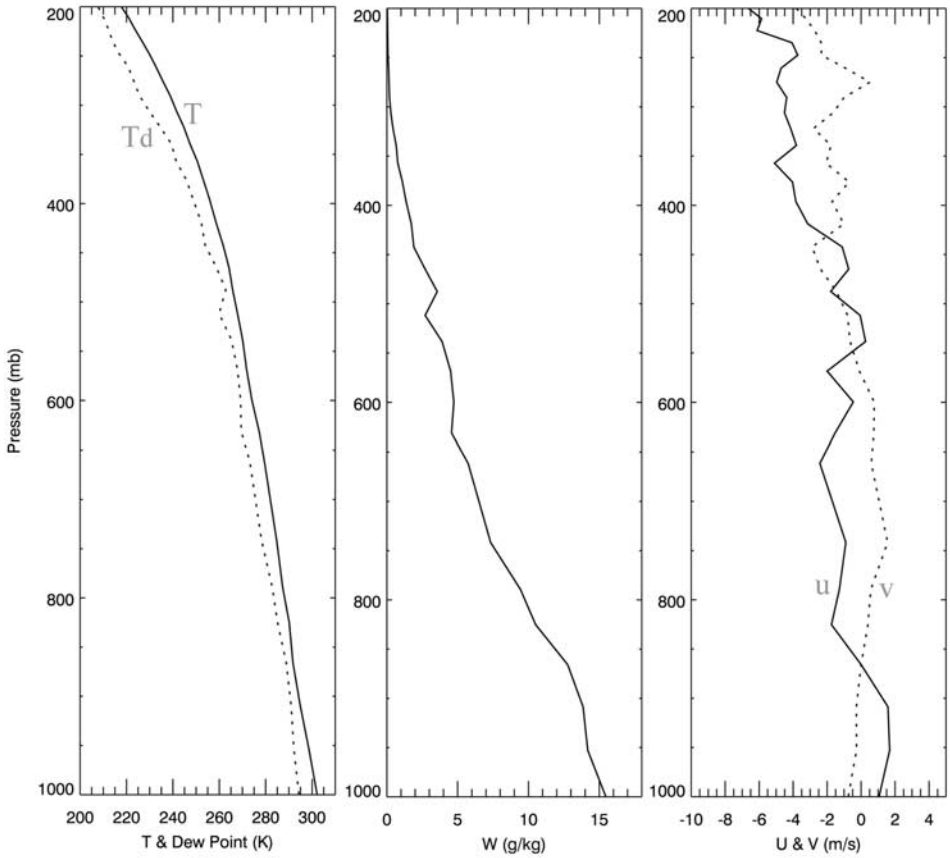


**Figure 1.** Initial profiles of temperature (*T*), dew point (*Td*), water vapor mixing ratio (*w*), and horizontal winds *u* and *v* in Houston at 11:58 am local time.

the C-case has the same configuration as the P-case, except that the aerosol concentration is only 10% of the P-case. The M-case has the marine aerosol composition of NaCl and a size distribution taken from *Khain et al.* [2005]; the total aerosol concentration is about 400 $cm^{-3}$, less than that in the C-case, which is about 3000 $cm^{-3}$. Figure 2 presents the initial aerosol size distributions for the three aerosol cases. The M-case has large aerosol particles, but lacks small particles. The number concentrations of activated aerosols at 1% supersaturation for the P-, C-, and M-cases are 4415, 552, and 228 $cm^{-3}$, respectively. Additional simulations relevant to the continental conditions are also conducted by varying the aerosol concentration from 550 to $2 \times 10^5$ $cm^{-3}$ with 15 different initial values, to explore the responses of convective clouds to changes in aerosol number concentrations. Measurements reveal a large variation in the aerosol concentration over the Houston area, with the highest concentration approaching $10^5$ $cm^{-3}$ [*Fan et al.*, 2006]. The model configurations similar to the P-case (base run) are employed for all 15 simulations and the shapes of aerosol size distribution do not change. An exponential decrease of aerosol concentrations with height is used as the initial condition at $t = 0$: $N_0 = N_0\ (z = 0)\ \exp((z - z_0)/\Delta z)$, where $z_0$ = 2.0 km and $\Delta z$ = 1.2 km, which were obtained from the CMAQ simulations [*Fan et al.*, 2006]. The concentration of ice nuclei is calculated from the supersaturation with respect to ice ($S_{ice}$), as discussed by *Meyers et al.* [1992]. In our study, we assume that CCN participating in droplet nucleation do not serve as ice nuclei. The upper limit for supersaturation with respect to ice is set for utilization of parameterization formula of Meyers et al. to cap the ice heterogeneous nucleation.

[9] The impact of relative humidity (RH) on cumulus cloud development is evaluated for the three aerosol cases,

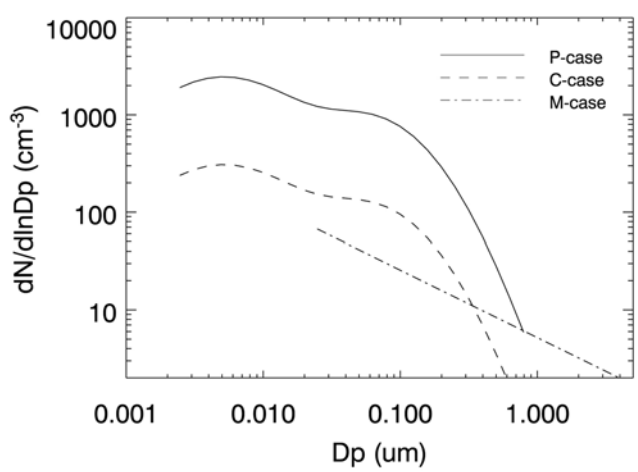


**Figure 2.** Initial size distributions for polluted (solid line), clean continental (dash line) and marine aerosol cases (dash dotted line).

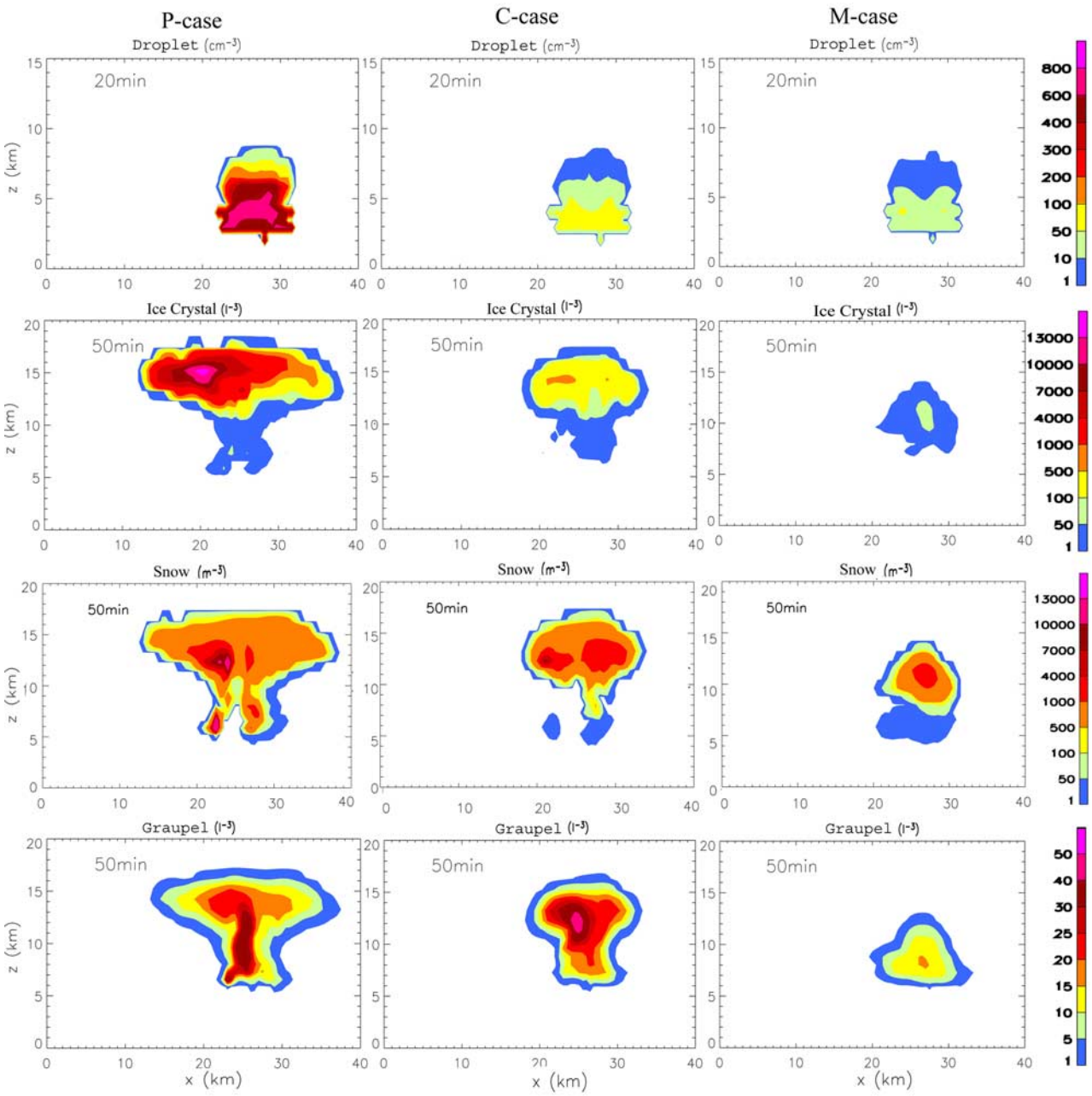


**Figure 3.** 2-D fields of number concentrations of cloud droplet, ice crystal, snow, and graupel for the P- (left), C- (middle) and M-cases (right) at the developing stages.

i.e., P-, C-, and M-cases. In each case, four RH conditions of 40, 50, 60 and 70% at the surface are considered, with 40 and 70% RH representing dry and humid conditions, respectively. This RH range is representative of the surface moist conditions in the Houston region during the early afternoon hours. The RH in the vertical levels varies with the surface RH accordingly (with a same factor). For example, the RH is about 99% at 1.5 km for the 70% surface RH condition.

[10] The triggering of convection was made using the warm bubble method [*Fan et al.*, 2007], and was similar in all simulations. The dynamic time step is 6 s in all the simulations. To survey the responses of modeled deep convective clouds to the changes in aerosol and RH conditions, we perform statistical analyses of the mean model variables. The cloud area mean (area-mean) and the population mean (p-mean) of a variable are calculated similarly to *Wang* [2005]. The area-mean corresponds to the averaged value over a specific region at an output time step, while the p-mean represents the averaged value over all qualified grids and during the entire simulation period.

## 3. Results and Discussion

### 3.1. Effects of Aerosol Types: Continental vs. Marine

[11] The two-dimensional fields of the number concentrations of cloud droplets at 20 min and ice particles at 50 min for the P-, C-, and M-cases are presented in Figure 3.

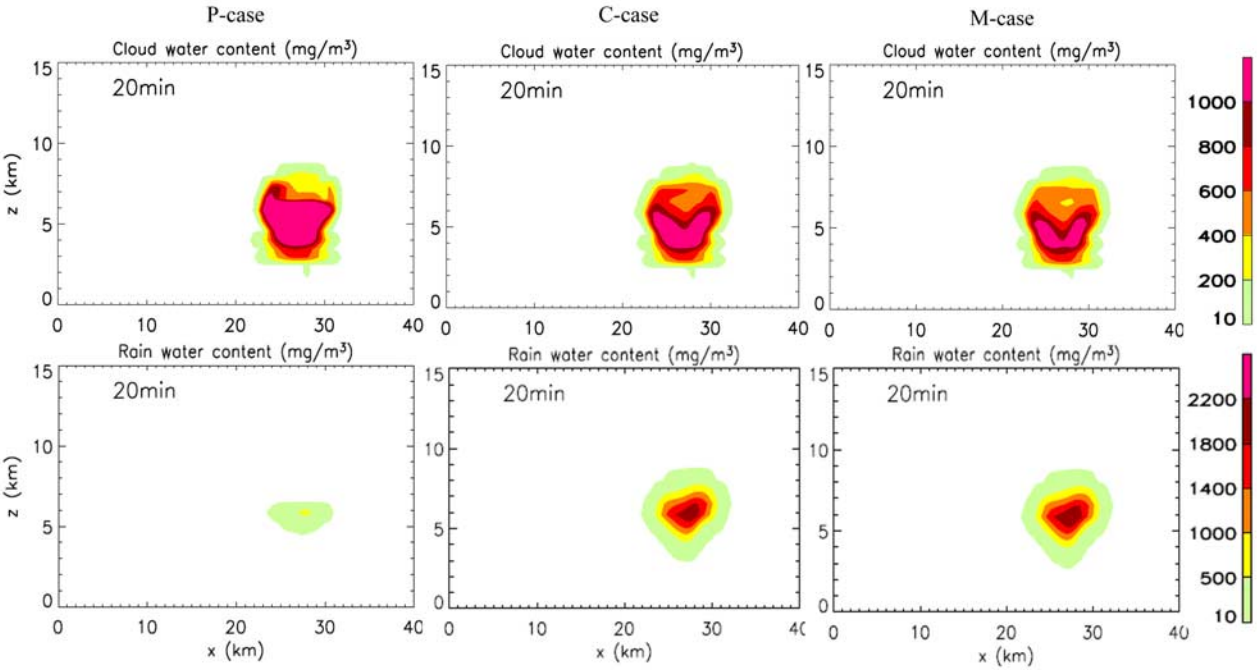


**Figure 4.** 2-D fields of CWC and RWC for the P- (left), C- (middle) and M-cases (right) in the developing stage at 20 min.

At about 20 min, the cloud droplet number concentration reaches a maximum value. The largest difference in the ice particle concentration among the three cases occurs at 50 min. Figures 4 and 5 illustrate the mass concentrations of hydrometeors at the developing stages. The most noticeable difference in Figure 3 is that the P-case predicts significantly higher number concentrations of cloud droplets, ice crystals and snow than the C- and M-cases. Also, the cloud anvil (the coverage of ice phase) at 50 min is the largest for the P-case, likely because of more droplet condensation at a higher droplet number concentration and hence a stronger convection [*Khain et al.*, 2005]. The instant maximum updraft velocity during the developing stage is 16.4 m/s in the P-case, and only 10.4 in the C- case and 8.0 m/s in M-cases. The large anvil can also be explained by the smaller cloud droplets in the P-case that ascend to the higher levels, in contrast to larger raindrops formed in the C- and M-cases that settle down. The p-mean droplet effective radius in the P-case is 8.3 $\mu$m, much smaller than those in the C- and M-cases (13.6 and 14.5 $\mu$m, respectively). The more droplet condensation is responsible for the higher cloud water content (CWC) in the P-case (Figure 4). The higher droplet concentrations in the P-case extend up to the 7-km level (Figure 3), indicating a less efficient coalescence compared with the C- and M-cases, in which the droplet concentrations decrease more rapidly with height because of more efficient droplet collisions and raindrop formation. The higher rainwater content (RWC) for the C- and M-cases in Figure 4 reflects more efficient raindrop formation; the higher supersaturation in both cases leads to faster condensation growth of droplets, yielding a larger droplet size, and therefore more efficient coalescence. The values of the area-mean supersaturation at 20 min in the P-, C-, and M-cases are 0.016, 0.022 and 0.033%, respectively. The vertical velocities at the cloud base in P- and M-cases at 20 min are similar, about 1-2 m/s. Within 2-5 km above the cloud base, the vertical velocity is about 4-6 m/s in the P-case and about 3-5 m/s in the M-case. The raindrops form at about the same level in the P- and M- cases at 20 min because there is no significant difference in vertical velocity between them, probably attributing to the same warm bubble initialization. The increase of cloud droplet concentration and CWC in the polluted air is consistent with previous observations in warm cumulus clouds [*Rosenfeld*, 2000; *Kaufman and Koren*, 2006] and model simulations for deep convective clouds [*Khain and Pokrovsky*, 2004]. Ice crystals in the P- and C-cases are primarily distributed above the 10-km level, indicating that they are mainly formed by homogeneous freezing. However, in the M-case much less droplets reach the freezing level because of a much weaker convective strength, lack of small aerosol particles, and efficient growth into raindrops. The much higher supersaturation with respect to ice ($S_{ice}$) in the M-case causes more efficient ice growth by deposition, contributing to the higher mass concentrations of snow (Figure 5). Alternatively, more efficient collision of ice-ice due to larger droplet sizes also contributes to the higher snow mass. Since ice crystals are rapidly transformed into snow and graupel, the ice crystal number and mass concentrations are low in the M-case (Figures 3 and 5). The P-case predicts higher graupel number and mass concentrations than the M-case (Figures 3 and 5) because of more extensive riming at higher droplet number concentrations. The graupel concentrations in the C-case are comparable to that in the P-case, attributable to more efficient drop-ice collision in the C-case.

[12] The radar reflectivity at the developing (~50 min) and mature (~120 min) stages is depicted in Figure 6 for the three cases. The more efficient production of rainwater,

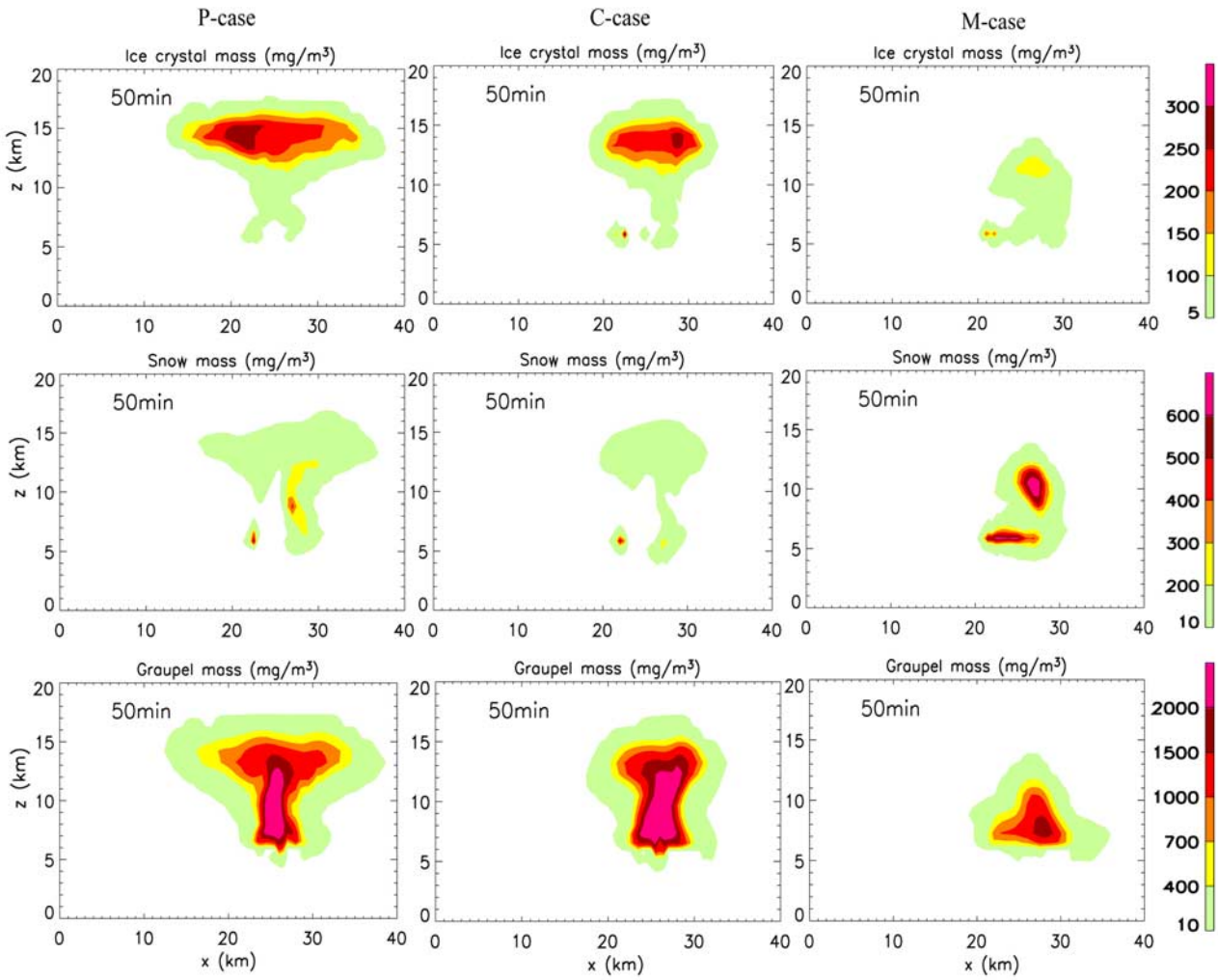


**Figure 5.** 2-D fields of mass concentrations of ice crystal, snow and graupel for the P- (left), C- (middle) and M-cases (right) in the developing stage at 50 min.

snow and graupel at 50 min is responsible for the more intensive radar reflectivity in the C and M-cases. At the mature stage, M-case predicts stronger radar reflectivity than the P- and C- cases.

[13] Figure 7a shows the temporal evolution of the maximum updraft velocity for the three cases. In the developing stage from 15 min to about 50 min, the P-case predicts up to 45% higher maximum updraft velocity than the C-case, while the C-case predicts up to 60% higher than the M-case. The largest updraft velocity for the P-case is attributed to the highest droplet condensation due to the highest droplet number concentration. During the intermediate stage from about 50 min to 90 min, the maximum updraft velocity is the highest in the M-case, with the maximum difference of over 40%. The maximum convective strength occurs at about 40, 45 and 60 min in the P-, C-, M-cases, respectively. The convection develops faster in the P-case due to much more latent heat release from droplet condensation. The cloud in the M-case develops slower and the updraft velocity reaches its maximum about 20 min later relative to the P-case (Figure 7a). The downdraft resulted from the fallout of warm rain at the early stage in the M-case can work as an increase in the buoyancy at the later stage, possibly contributing to the strong convection during 60-90 min. Figure 8 shows the cloud fields in the M-case at 65 min when the cloud intensity is near the maximum. The strong convection at about 60 min is responsible for the high mass concentrations of ice particles. The high water content (primarily rainwater) above 5 km indicates strong melting precipitation. The cloud from 60 to 90 min is from the primary cell and the ice processes are enhanced by the delayed convection.

[14] In Figure 6, the M-case predicts the most intensive total radar reflectivity among the three cases at 120 min because of the strongest convection from 60 to 90 min (Figure 7a). The high total radar reflectivity is reflected in the high radar reflectivity of ice crystal and snow in the M-case. The calculated radar reflectivity for a specific hydrometeor increases with the mass concentration and decreases with the number concentration. Figure 9 illustrates the mass concentrations of hydrometeors at 120 min. The mass concentrations of ice crystals and snow in the M-case are higher due to higher $S_{ice}$. The formation of ice crystals at the levels over 15 km in the P- and C-cases is primarily through homogeneous freezing. In the P-case, more droplets are transported to these levels with stronger

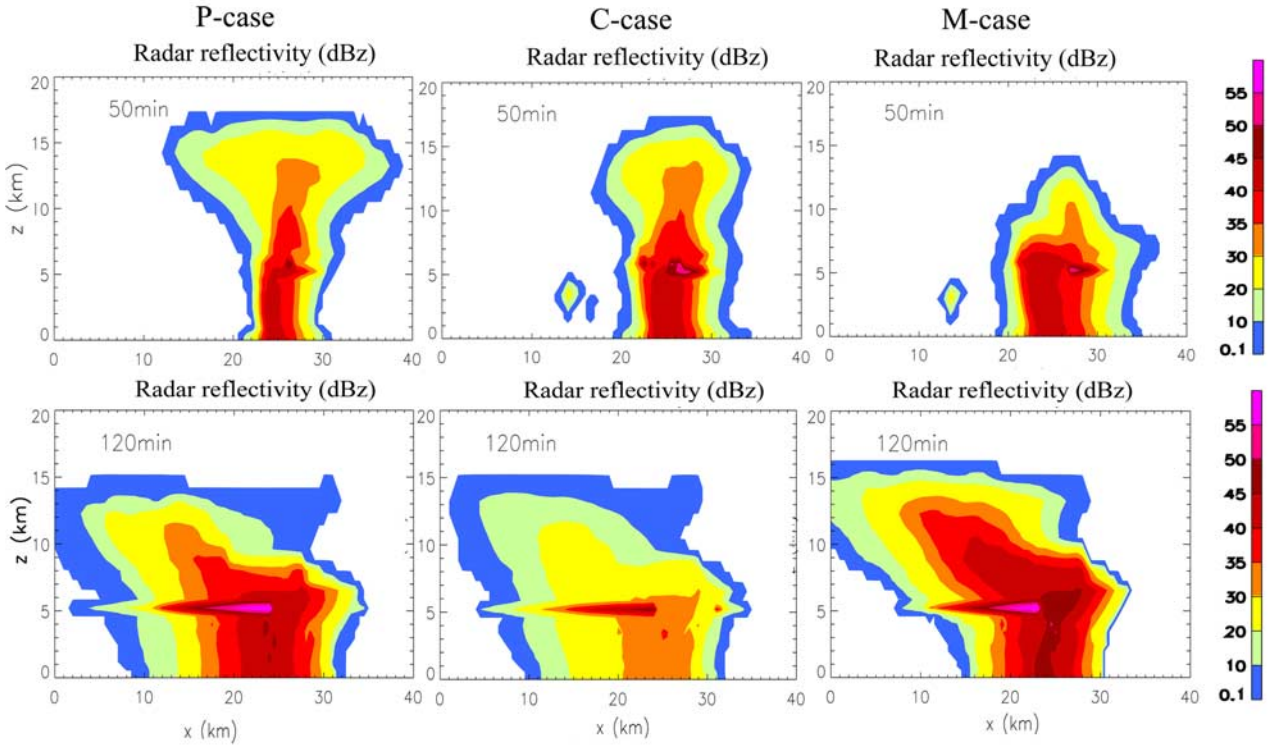


**Figure 6.** The total radar reflectivity of P- (left), C- (middle) and M-cases (right) in the developing stage at 50 min and mature stage at 120 min.

convection and higher droplet number concentrations, leading to higher ice crystal concentrations than those in the C-case (Figures 3 and 5). For the low concentration of supercooled droplet (M-case), the ice crystal formation is determined from the parameterization formula by *Meyers et al.* [1992], where the ice nuclei concentration is proportional to $S_{ice}$. The high $S_{ice}$ in the M-case leads to high ice crystal formation according to the parameterization and also efficient diffusion growth of ice crystals, yielding the high mass concentrations of ice crystals (Figure 9). The p-mean $S_{ice}$ from 90 to 120 min is 0.047, 0.062, and 0.101% for the P-, C-, and M-cases, respectively. The production mechanisms of snow and graupel correspond to ice-ice and drop-ice collisions, respectively. Efficient ice-ice collisions in the M-case due to larger sizes of ice particles resultant from the higher supersaturation lead to the much higher snow concentration. The much lower graupel mass concentration in the M-case than the other two cases at 120 min (Figure 9) is mainly because of the less graupel production at a much lower supercooled droplet concentration.

[15] A comparison of cloud macrophysical properties is shown in Table 1. The P-case predicts almost two times larger cell size and about 60 min longer cell lifetime than the C-case. The cell lifetime and size are defined from the radar reflectivity that is greater than 30 dBz. Also, the total rain over the entire domain is higher in the P-case than that in the C-case. As shown in Figure 7b, the time-dependence of the area-mean accumulated rain reveals that the secondary clouds contribute to the precipitation significantly in the P-case, but not in the C- and M-cases. The enhanced melting precipitation rate and the stronger secondary con-

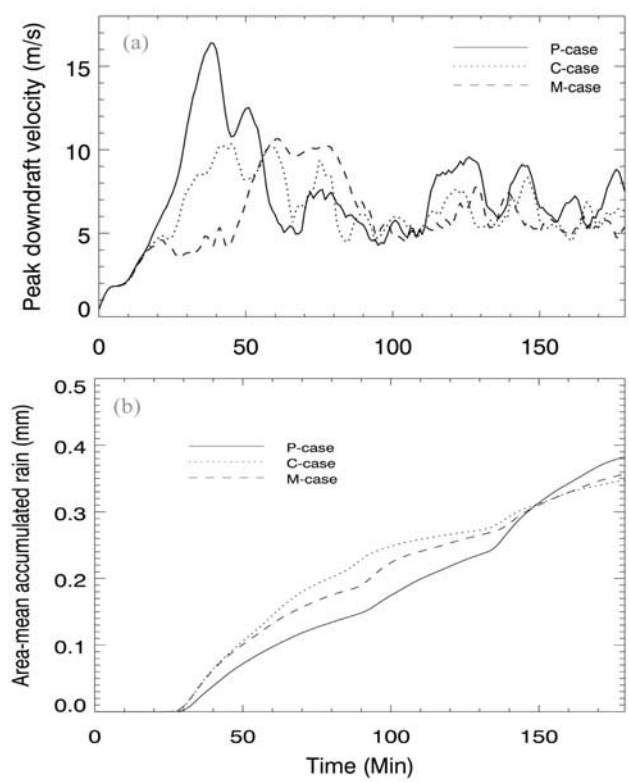


**Figure 7.** (a) Time dependence of the maximum updraft velocity and (b) the area-mean accumulated rain for the P- (solid line), C- (dotted line) and M-cases (dashed line).

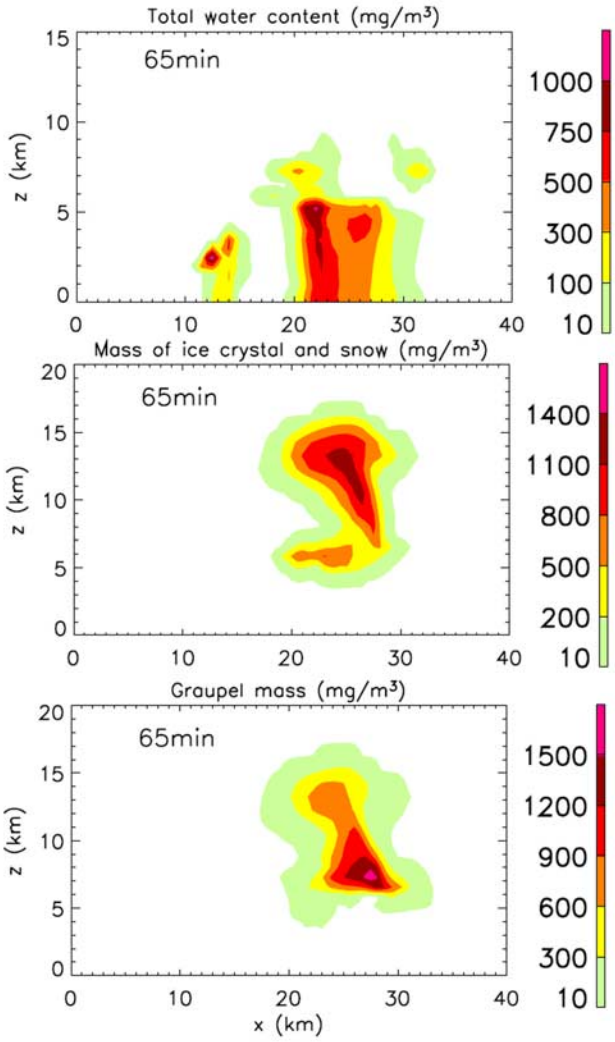


**Figure 8.** The cloud fields in the M-case at 65 min when the cloud intensity is near the maximum.

vection caused by the higher aerosol concentrations primarily contribute to the increased precipitation in the P-case. The stronger updraft in the P-case enhances the upward transport of liquid drops and retards sedimentation of ice particles. The former effect is responsible for rapid formation of ice particles and the latter decreases the number of ice particles settling down to the warm region. Moreover, the stronger updraft elevates the glaciation level where large ice particles are formed from higher collision efficiencies for aggregation. Also, more extensive riming of ice particles in the P-case is due to the much higher supercooled droplet number concentration. All those result in more melting precipitation, longer cell lifetime, larger cell size, and stronger secondary clouds in the P-case than in the C-case. The total domain precipitation for the P-case is higher than that for the C-case, suggesting an enhanced precipitation with increasing aerosols. It agrees well with the results obtained by *Khain et al.* [2005], in which deep convection under different aerosol concentrations and RH has been simulated. The humid environment and large surface heating in the Houston region [*Fan et al.*, 2007] likely create favorable thermodynamic and dynamic conditions for a positive aerosol-precipitation relation. Our modeled precipitation enhancement is in agreement with field measurements around heavily polluted coastal urban areas in this region [*Shepherd and Burian*, 2003].

[16] The total domain rain for the M-case is comparable to that for the P-case. The M-case has a longer cell lifetime than the P-case, due to significant delay in convective development. The dominance of low-density snow in the ice phase from more efficient deposition growth of ice crystals in the M-case corresponds to a much lower downdraft velocity relatively to graupel, leading to a longer resident time above freezing level. Similarly, the cell size in the M-case is close to that in the P-case. The aerosol size and distribution do not affect precipitation significantly here, since the clouds are triggered by a strong thermodynamic forcing (warm bubble) and water vapor can be transported to above freezing level in all three cases, contributing to melting precipitation. This dynamic effect on precipitation overwhelms the microphysical effect determined from aerosol properties (type, size and concentration). Our simulations of the cloud development, size, and lifetime in the M-case are different from those reported previously [*Khain et al.*, 2005], in which the initial thermodynamic conditions including temperature and water vapor profiles characteristic of a marine environment were applied. The non-monotonic features of the cloud size, cloud lifetime and cloud coverage with varying aerosol concentrations have been found for warm cumulus clouds by *Jiang et al.* [2006] and *Xue and Feingold* [2006].

### 3.2. Effects of Initial Aerosol Concentration

[17] The responses of the p-mean number and mass concentrations of hydrometeors to the increase of the initial aerosol concentration in the continental aerosol environment are presented in Figures 10 and 11, respectively. It is evident from Figure 10a that the number concentration of cloud droplet increases with increasing aerosol concentrations in the range of 550 to $2 \times 10^5$ cm$^{-3}$. For the case with the total aerosol concentration of $2 \times 10^5$ cm$^{-3}$, the p-mean droplet concentration is about $2 \times 10^3$ cm$^{-3}$, but the instant droplet concentration is up to $6 \times 10^3$ cm$^{-3}$ at the developing stage of the cloud. The droplet concentration can be limited by the growth of CCN in the very high aerosol concentration cases. The p-mean number concentration of ice crystal also increases with aerosol (Figure 10b), but the change of graupel number concentration is not monotonic (Figure 10c). The p-mean CWC and graupel mass concentration increase with the aerosol concentration of less than about $1.5 \times 10^4$ cm$^{-3}$ (referred to as "low-aerosol cases"), as shown in Figure 11a and 11d, respectively. The mass concentrations of all hydrometeors become much less sensitive to the aerosol concentration above $1.5 \times 10^4$ cm$^{-3}$ (referred to as "high-aerosol cases"). The lower RWC and graupel mass concentration (Figures 11b and 11d) in the high-aerosol cases than those in the low-aerosol cases are primarily due to the less efficient collisions of drop-drop and drop-ice (graupel). The p-mean RWC is not very sensitive to aerosol probably because the increase of the melting precipitation compensates with the decrease of warm rain processes with increasing aerosols.

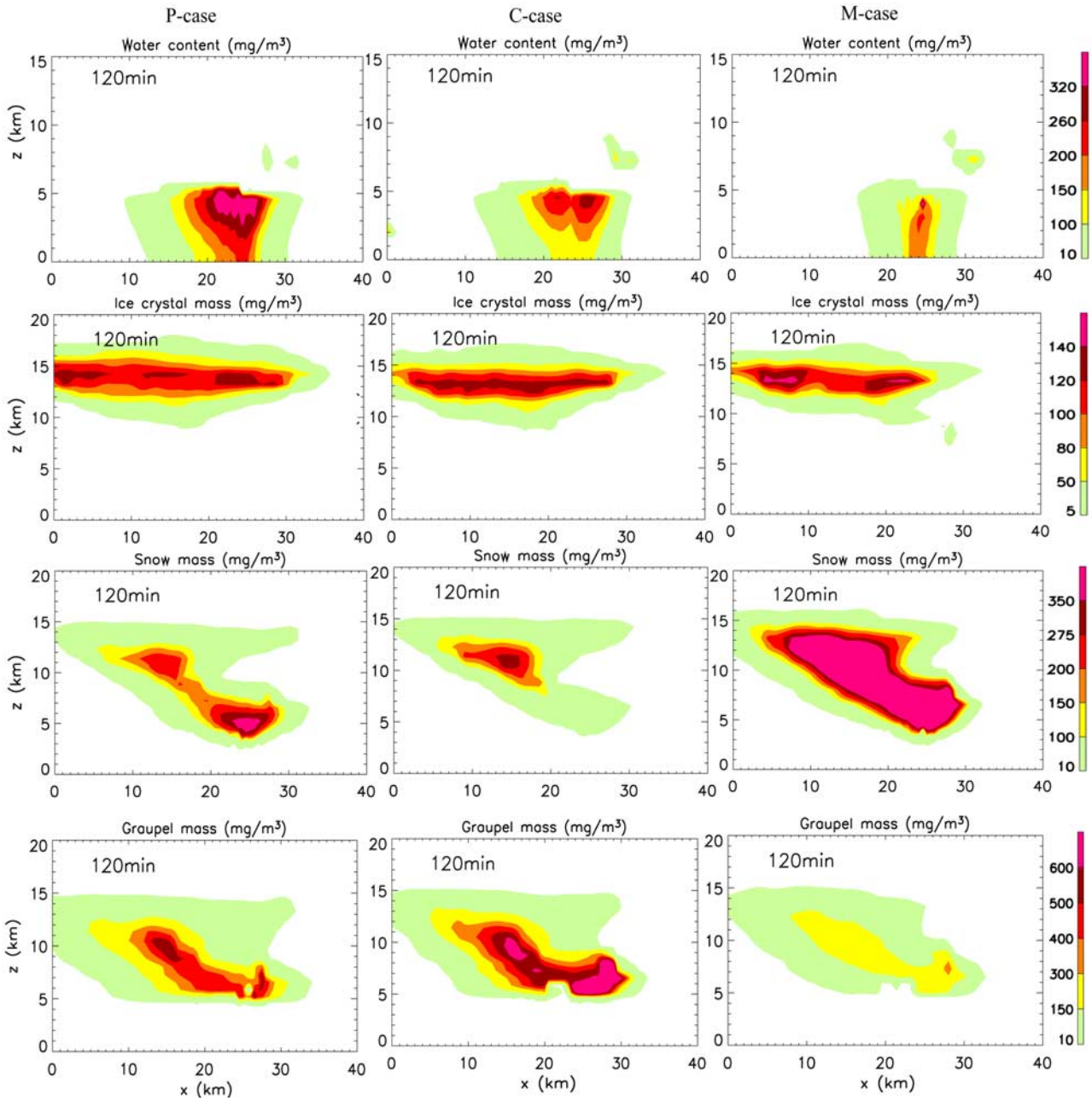


**Figure 9.** 2-D fields of mass concentrations of liquid water, ice crystal and snow for the P- (left), C- (middle) and M-cases (right) in the mature stage at 120 min.

[18] In contrast, to the cloud water content and droplet number concentration, the p-mean cloud droplet size decreases with increasing aerosols (Figure 12a). From the aerosol number concentrations of 550 to $2 \times 10^5$ cm$^{-3}$, the p-mean effective radius of cloud droplets is reduced by 70%. In the high-aerosol cases, the reduction in the effective radius of cloud droplets with increasing aerosol becomes less significant, which appears to be consistent with the observation from satellite for warm clouds [*Feingold et al.*, 2001; *Bréon et al.*, 2002]. The latent heat release associated with the condensation of cloud droplets enhances the updraft velocities in the cloud (Figure 12b), although the convection is less sensitive to aerosols in the high-aerosol cases. As shown in Figure 12c, the secondary clouds are stronger with increasing aerosols except for the extremely high aerosol cases (over about $5 \times 10^4$ cm$^{-3}$), in which the convection is suppressed because of the very low supersaturation resulting from droplet condensation.

[19] The response of precipitation to increasing aerosols is not monotonic (Figure 13a). The total precipitation in the

**Table 1.** Comparisons of the Results from P-, C- and M-cases

| | P-case | C-case | M-case |
|---|---|---|---|
| Max. radar reflectivity (dBz) | 61.1 | 58.4 | 62.7 |
| Cell lifetime (min) | 140 | 80 | 150 |
| Cell size (>30 dBz) (km) | 14 | 7.5 | 12 |
| Total domain rain (mm) | 366.8 | 356.3 | 364.1 |

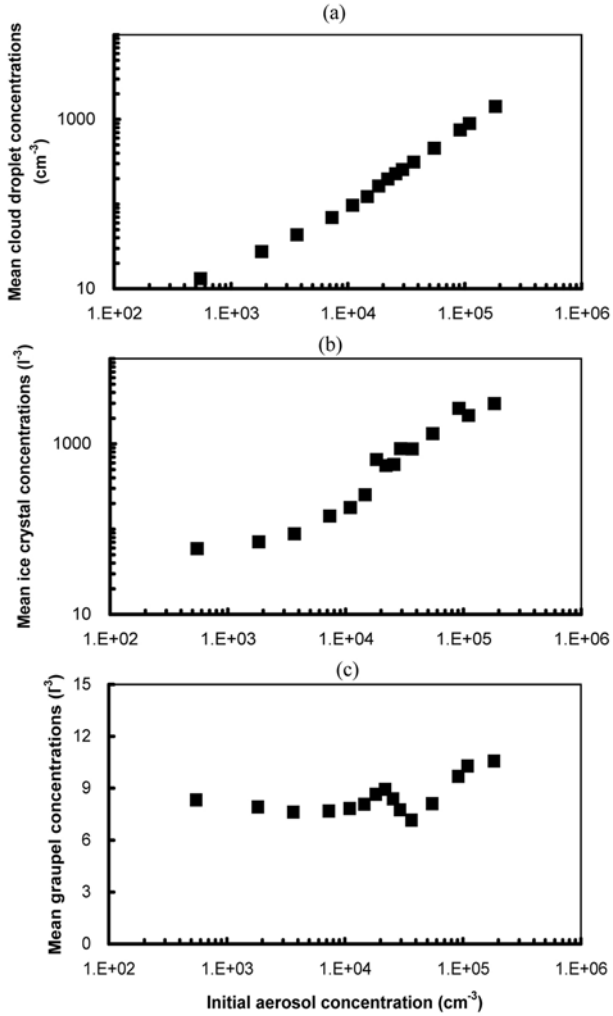


**Figure 10.** P-mean number concentrations of (a) cloud droplet, (b) ice crystal, and (c) graupel with increasing aerosols.

entire domain increases with aerosols except for the extremely high aerosol cases. The enhanced total precipitation with increasing aerosols is primarily due to enhanced melting rain rates and stronger secondary clouds. The total precipitation significantly decreases with increasing aerosols in the extremely high aerosol cases, likely because of suppressed convection from depletion of water vapor and inefficient coalescence for small droplet sizes. There is a slight rain delay with increasing aerosol (Figure 13b). In our simulations with increasing aerosols, the aerosol sizes remain invariant, and hence the sizes of activated aerosols are invariant. A strong warm bubble initialization for all the cases probably reduces the delay of initial rain.

[20] The present results that cloud number concentrations, cloud water, cloud coverage, and precipitation increase while the cloud droplet size decreases with aerosol concentration, are consistent with the study of deep convection conducted by *Wang* [2005]. However, in our study the increases in cloud properties are found to reach a maximum value at a certain aerosol concentration. The cloud properties then become insensitive or decrease with further increasing aerosol concentrations. The range of the aerosol concentration employed in the work of *Wang* [2005] corresponds to the concentration at the low-aerosol cases used in our study. In addition, the increase in ice crystal number concentration is much more sensitive to aerosol concentration in this study than that in the work of *Wang* [2005], likely caused by the different ice microphysics employed.

### 3.3. Effects of Relative Humidity (RH)

[21] To survey the aerosol effects on cloud properties under different RH conditions, we conduct simulations for the three aerosol scenarios, i.e., P-, C- and M-cases, at four RH conditions of 40, 50, 60 and 70% at the surface. The

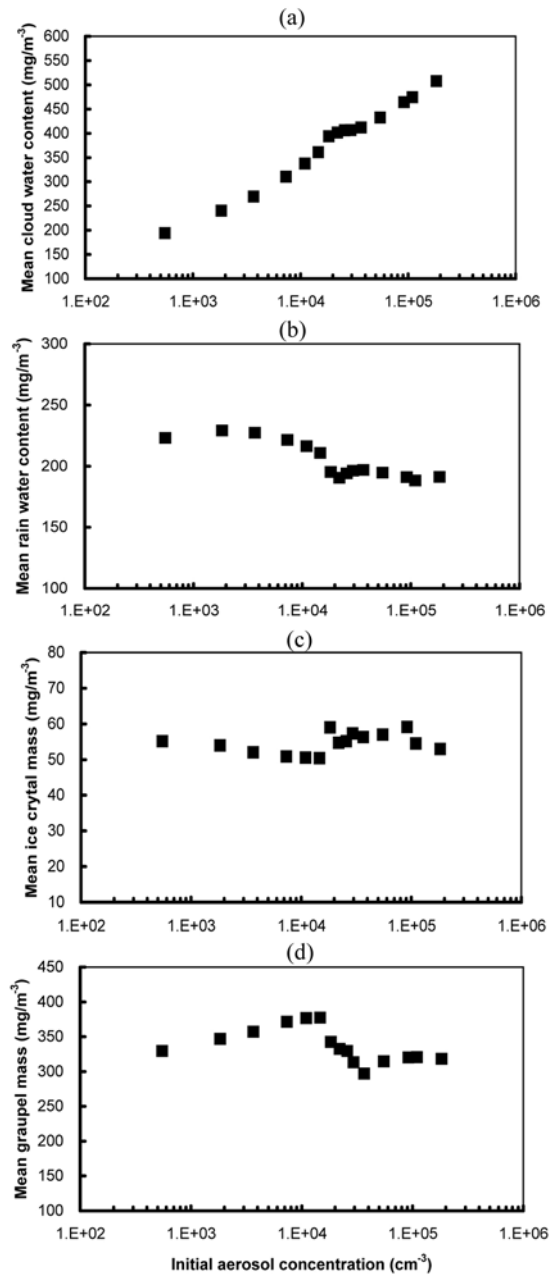


**Figure 11.** P-mean mass concentrations of (a) cloud droplet, (b) rain drop, (c) ice crystal, and (d) graupel with increasing aerosols.

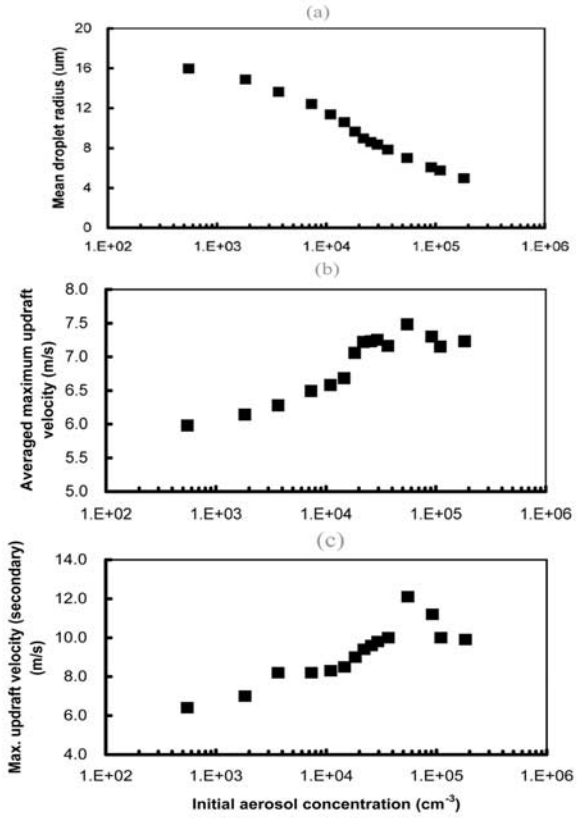


**Figure 12.** (a) P-mean effective droplet radius, (b) averaged maximum updraft velocity over the simulation time, and (c) the maximum updraft velocity of the secondary clouds with increasing aerosols.

cloud development is dramatically affected by relative humidity, because of a significant change in the CAPE. The CAPE increases dramatically with increasing RH, with the values of 0.0, 19.0, 960.0 and 2840.0 J $kg^{-1}$ at the 40, 50, 60 and 70% surface RH conditions, respectively. The fields of mass concentrations of hydrometeors for the P-case at 50, 60 and 70% RH are shown in Figure 14. At 40% RH only limited shallow warm cumulus develops. The mass concentrations of hydrometeors dramatically increase with increasing RH, as is the case for the number concentrations of hydrometeors (not shown). The cloud base height decreases significantly with increasing RH, as reflected from the profile of cloud water content. Ice phase processes are limited at lower RH (40 and 50% surface RH), but are greatly enhanced at higher RH (60 and 70% surface RH). At 70% RH, the maximum updraft is 42.5 m/s, corresponding to extremely strong convection because of very large CAPE. The clouds at 70% RH appears to be too strong, likely attributable to the coarse vertical resolution of the model upper layers. In addition, cloud development is about 15 min earlier at 70% RH than that at 50% RH. The level of the ice phase is significantly elevated and the cloud anvil is greatly expanded when RH increases from 50 to 70% RH as shown in Figure 14, due to the significant increase of CAPE.

[22] The aerosol effect on the cloud microphysical properties is strongly dependent on RH: the effect is negligible in relatively dry air and becomes much pronounced in humid air. The p-mean mass concentrations of hydrometeors for the P-, C- and M-cases at different RH conditions are depicted in Figure 15. Generally, the hydrometeor mass concentrations increase with RH and the aerosol effect on CWC is evident (Figure 15a). The p-mean RWC increases with RH as shown in Figure 15b, but it is higher in the C-case than that in the P-case, primarily because of the more efficient coalescence relating to larger droplet sizes. As shown in Figure 15c, for all three aerosol cases, the ice crystal mass concentration increases dramatically when RH increases from 50 to 70%, but there is little difference between 40 and 50% RH. The aerosol effect on ice crystal mass is significant only in humid air. The p-mean graupel mass concentration increases with RH and the aerosol effect on graupel is more evident at the higher RH (Figure 15d). The C-case predicts graupel mass comparable to the P-case. The much lower mean graupel mass in the M-case is caused by the much lower droplet number concentration due to the very low aerosol particles. The small differences in cloud properties between 40 and 50% RH are explained by little difference in CAPE.

[23] As shown in Figure 16a, when RH increases from 40 to 60% the p-mean effective droplet radius is not sensitive to RH, but very sensitive to aerosol. However, the droplet size is significantly larger at 70% RH than that at 60% RH. The P-case consistently predicts much smaller droplet size than C- and M-cases at all RH conditions. The droplet size is determined jointly by the number of nucleated droplets and supersaturation, which have opposite effects on the effective radius. The cloud dynamics changes most noticeably with RH and also with aerosols to a lesser extent. The maximum updraft velocity increases with RH due to increasing CAPE (Figure 16b). The aerosol effect on the

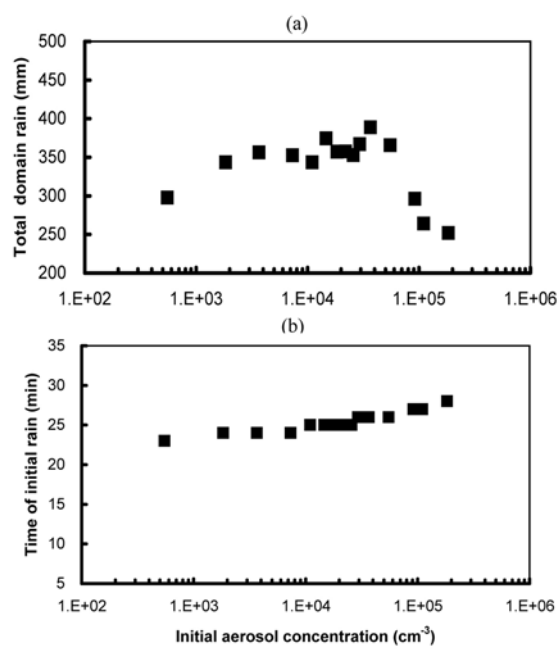


**Figure 13.** (a) Total domain precipitation, and (b) time of initial rain formation with increasing aerosols. The total domain precipitation is the sum of accumulated rain of every grid.

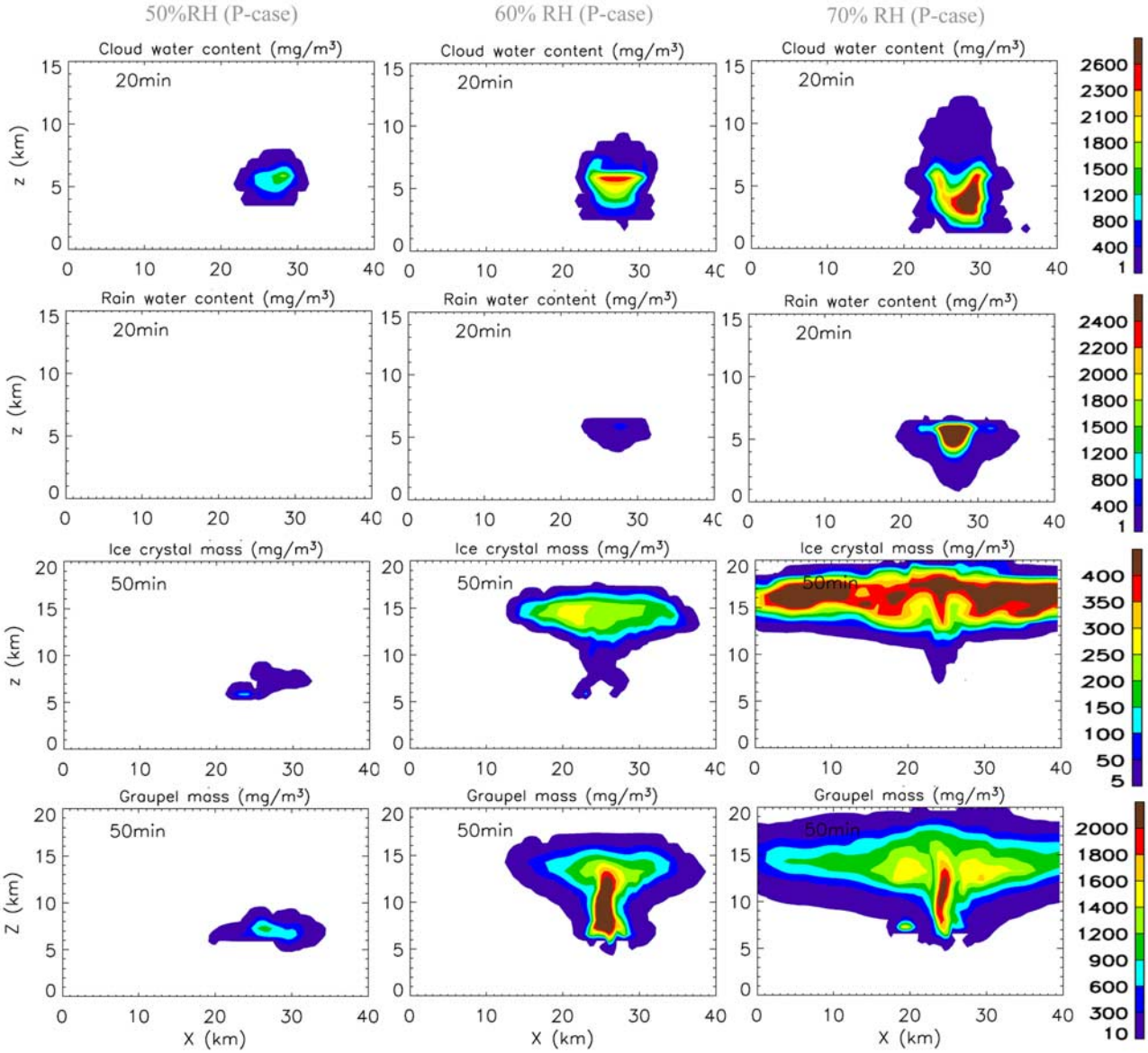


**Figure 14.** 2-D fields of CWC, RWC and mass concentrations of ice crystal and graupel for the P-case at 50 (left), 60 (middle) and 70% (right) RH.

convective strength is only significant in relatively humid air, i.e., at 60 and 70% surface RH. More water vapor can be condensed by aerosols in humid air, leading to more significant influences of aerosols on cloud microphysical and dynamic properties.

[24] The response of precipitation to RH for the three aerosol cases is shown in Figure 17. The aerosol effect on the maximum rain rate is most significant under the moist conditions, and the M-case predicts significantly lower maximum rain rate in the humid air (70% RH) (Figure 17a). The response of accumulated rain to RH has the similar relationship with the rain rate as shown in Figure 17a. The larger maximum rain rate in the P-case relative to the M-case is consistent with the results reported by *Lynn et al.* [2005b]. As shown in Figure 17b, the rain delay is very sensitive to RH, but not very sensitive to aerosol under the same initial thermodynamic conditions. *Khain et al.* [2005] found a significant delay in the onset of precipitation in the continental cloud compared with the maritime cloud. In our simulations the same sounding and warm bubble initialization determine an initial strong convective development and hence a less delay in precipitation [*Fan et al.*, 2007].

## 4. Summary and Conclusion

[25] In this paper the effects of composition and concentration of aerosols and the relative humidity on microphysics and dynamics of cumulus clouds characteristic of the coastal city of Houston, Texas have been evaluated using a two-dimensional spectral-bin cloud model. Our results show that for polluted continental, clean continental, and marine aerosol types at 60% surface RH the cloud properties are considerably influenced by the aerosol type and concentration. Under the same initial dynamic and thermodynamic conditions, the maritime aerosol results in more intensive

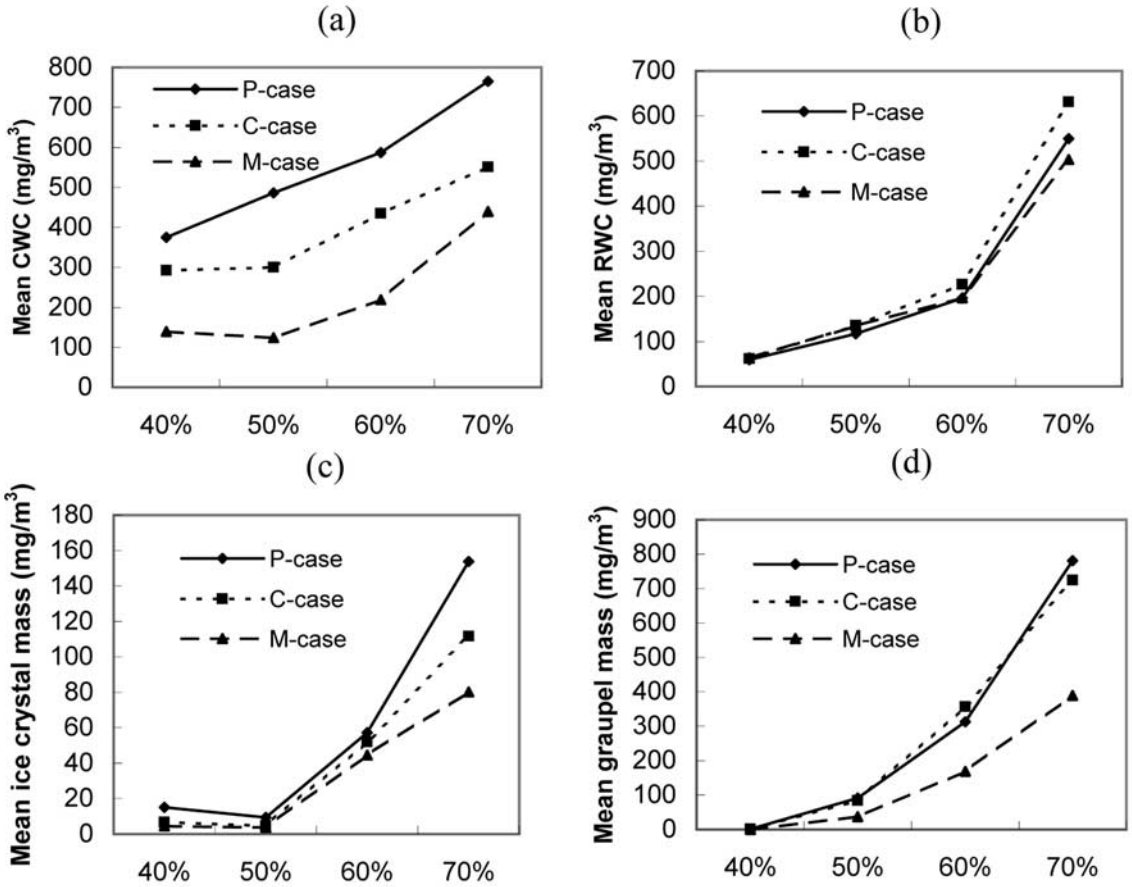


**Figure 15.** P-mean mass concentrations of (a) cloud droplet, (b) rain drop, (c) ice crystal, and (d) graupel for the P- (solid), C- (dotted) and M-cases (dash) at the different RH conditions.

radar reflectivity in both developing and developed stages than the continental aerosol in polluted air. For the continental case, the increase of initial aerosol concentration generally leads to a stronger convection. The most noticeable effect of increasing aerosol is the increases of the cloud droplet number concentration and cloud water content, but a decrease in the effective radius of cloud droplets. These changes lead to more extensive collection of small droplets

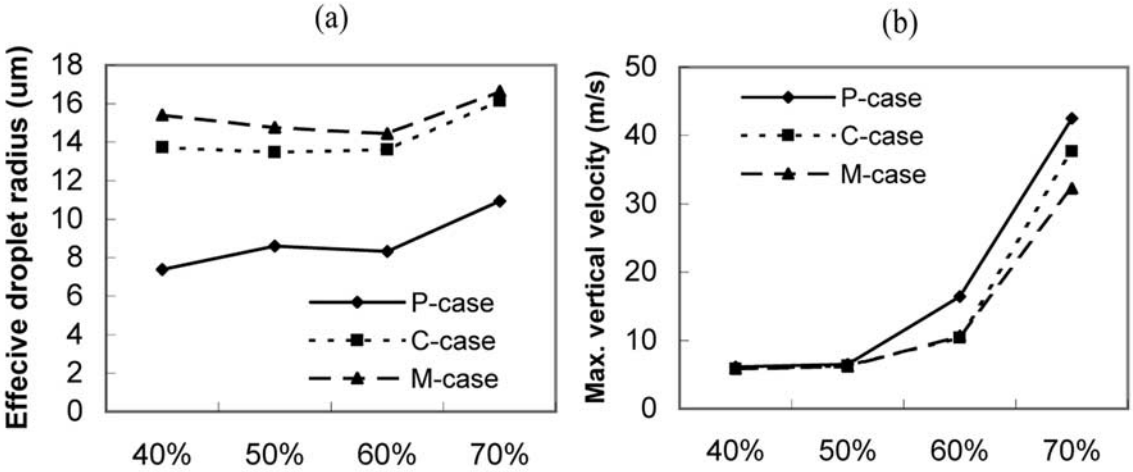


**Figure 16.** (a) P-mean effective droplet radii for the P- (solid), C- (dotted) and M-cases (dash) at the different RH, and (b) Maximum updraft velocity for the P- (solid), C- (dotted) and M-cases (dash) at the different RH conditions.

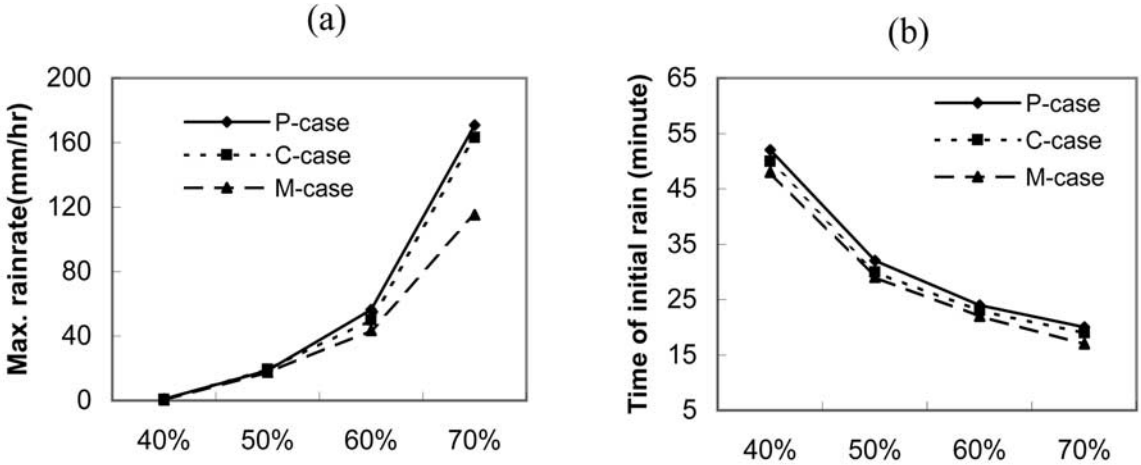


**Figure 17.** (a) Maximum rain rate, and (b) time of initial rain formation for the P- (solid), C- (dotted) and M-cases (dashed) at the different RH conditions.

by large drops and ice riming of supercooled droplets. The increase of the convection promotes the upward transport of the liquid drops, which leads to a faster formation of ice particles and retards ice particle sedimentation. Moreover, the stronger updrafts transport particles to higher levels where collision efficiencies are significantly higher and the rates of collisions in more turbulent flows are larger. Those microphysical and dynamical changes lead to the increase in the number and mass concentrations of hydrometeors, as well as greater cloud coverage.

[26] We show that the total amount of precipitation and rain rate increase with aerosols over this region, confirming measurements of precipitation enhancement reported previously [*Shepherd and Burian*, 2003]. More melting precipitation and stronger secondary clouds contribute to the enhanced precipitation with increasing aerosols. It agrees well with the results obtained by *Khain et al.* [2005], in which deep convection under different aerosol concentrations and RH has been simulated. Our simulations reveal that the aerosol effects on clouds and precipitation are dependent on cloud thermodynamic and dynamic conditions. The weak wind shear, the humid environment and large surface heating in the Houston region [*Fan et al.*, 2007] likely impact the aerosol-precipitation relation. The precipitation, however, decreases with increasing aerosol in the extremely high aerosol cases (over $5 \times 10^4$ cm$^{-3}$) due to suppression of convection from depleted water vapor and inefficient coalescence.

[27] The cloud development is dramatically affected by relative humidity. As RH increases from 40 to 70% at the surface, the cloud changes from shallow warm to deep convective types due to the significant increase of CAPE. From dry to humid air, the level of ice phase is significantly elevated and the cloud anvil is greatly expanded. The aerosol effects on the cloud microphysical properties and precipitation are found to be strongly dependent on RH: the effects are very significant in humid air (60-70% RH). Except for the very humid condition, the effective droplet radius is not sensitive to RH, but very sensitive to aerosol concentrations. The aerosol effects on the convective strength and the rain rate are significant in the humid air. The rain delay is found to be sensitive to RH, but not very sensitive to aerosol under the same initial thermodynamic conditions.

[28] This present study reveals that the cloud microphysical properties and precipitation depend critically on the aerosol types and concentrations under the same initial dynamic and thermodynamic conditions. In continental aerosol environments, the impact of aerosols on deep convective clouds is consistent with the Twomey effect, but the effect is non-linear. The effect of aerosols on cloud dynamics influences cloud macrophysical properties (i.e., cloud coverage, lifetime, and top height) significantly. The aerosol effect on deep convection is more pronounced in relatively clean air than in heavily polluted air, implying that aerosols may play a more important role in moist and clean marine environments [*Zhang et al.*, 2007]. The impacts of aerosols on cumulus clouds have major implications on radiative climate forcing.

[29] **Acknowledgments.** This study was partially supported by NSF (ATM-0424885). J. Fan was supported by NASA Headquarters under the Earth System Science (ESS) Fellowship. W.-K. Tao was supported by the NASA Headquarters Atmospheric Dynamics and Thermodynamics Program and the NASA Tropical Rainfall Measuring Mission (TRMM), and the Office of Science (BER), U.S. Department of Energy (No. DE-AI02-06ER64177). The authors were grateful to Dr. R. Kakar at NASA headquarters for assistance in this research. The three reviewers are greatly appreciated for valuable comments to improve this paper.

## References

Andreae, M. O., D. Rosenfeld, P. Artaxo, A. A. Costa, G. P. Frank, K. M. Longo, and M. A. F. Silva-Diaz (2004), Smoking rain clouds over the Amazon, *Science*, *303*, 1337–1341.

Bond, D. W., R. Zhang, X. Tie, G. Brasseur, G. Huffines, R. E. Orville, and D. J. Boccippio (2001), $NO_x$ production by lightning over the continental United States, *J. Geophys. Res.*, *106*, 27,701–27,709.

Bond, D. W., S. Steiger, R. Zhang, X. Tie, and R. E. Orville (2002), The importance of $NO_x$ production by lightning in the tropics, *Atmos. Envior.*, *36*, 1509–1519.

Bréon, F.-M., D. Tanré, and S. Generoso (2002), Aerosol effect on cloud droplet size monitored from satellite, *Science*, *295*, 834–838.

Fan, J., R. Zhang, G. Li, J. Nielsen-Gammon, and Z. Li (2005), Simulations of fine particulate matter (PM2.5) in Houston, Texas, *J. Geophys. Res.*, *110*, D16203, doi:10.1029/2005JD005805.

Fan, J., R. Zhang, D. Collins, and G. Li (2006), Contribution of Secondary Condensable Organics to New Particle Formation: A Case Study in Houston, Texas, *Geophys. Res. Lett.*, *33*, L15802, doi:10.1029/2006GL026295.

Fan, J., R. Zhang, G. Li, W.-K. Tao, and X. Li (2007), Simulations of cumulus clouds using a spectral microphysics cloud-resoving model, *J. Geophys. Res.*, *112*, D04201, doi:10.1029/2006JD007688.

Feingold, G., L. A. Remer, J. Ramaprasad, and Y. J. Kaufman (2001), Analysis of smoke impact on clouds in Brazilian biomass burning regions: An extension of Twomey's approach, *J. Geophys. Res.*, *106*, 22,907–22,922.

Feingold, G., H. Jiang, and J. Y. Harrington (2005), On smoke suppression of clouds in Amazonia, *Geophys. Res. Lett.*, *32*, L02804, doi:10.1029/2004GL021369.

Heymsfield, A., and G. M. McFarquhar (2001), Microphysics of INDOEX clean and polluted trade cumulus clouds, *J. Geophys. Res.*, *106*, 28,653–28,673.

Intergovernmental Panel on Climate Change (IPCC) (2001), *The Scientific Basis*, Cambridge Univ. Press, New York.

Jiang, H., and G. Feingold (2006), Effect of aerosol on warm convective clouds: Aerosol-cloud-surface flux feedbacks in a new coupled large eddy model, *J. Geophys. Res.*, *111*, D01202, doi:10.1029/2005JD006138.

Jiang, H., H. Xue, A. Teller, G. Feingold, and Z. Levin (2006), Aerosol effect on the lifetime of shallow cumulus, *Geophys. Res. Lett.*, *33*, L14806, doi:10.1029/2006GL026024.

Kaufman, Y. J., and I. Koren (2006), Smoke and pollution aerosol effect on cloud cover, *Science*, *313*, 655–658.

Khain, A. P., and A. Pokrovsky (2004), Simulation of effects of atmospheric aerosols on deep turbulent convective clouds using a spectral microphysics mixed-phase cumulus cloud model, Part II: Sensitivity Study, *J. Atmos. Sci.*, *61*, 2983–3001.

Khain, A. P., A. Pokrovsky, and I. Sednev (1999), : Some effects of cloud–aerosol interaction on cloud microphysics structure and precipitation formation: Numerical experiments with a spectral microphysics cloud ensemble model, *Atmos. Res.*, *52*, 195–220.

Khain, A. P., A. Pokrovsky, M. Pinsky, A. Seifert, and V. Phillips (2004), Simulation of effects of atmospheric aerosols on deep turbulent convective clouds using a spectral microphysics mixed-phase cumulus cloud model. Part I: Model description and possible applications, *J. Atmos. Sci.*, *61*, 2963–2982.

Khain, A. P., D. Rosenfeld, and A. Pokrovsky (2005), Aerosol impact on the dynamics and microphysics of deep convective clouds, *Q. J. R. Meteorol. Soc.*, *131*, 1–25.

Lei, W., R. Zhang, X. Tie, and P. Hess (2004), Chemical characterization of ozone formation in the Houston-Galveston area, *J. Geophys. Res.*, *109*, D12301, doi:10.1029/2003JD004219.

Li, G., R. Zhang, J. Fan, and X. Tie (2005), Impacts of black carbon aerosol on photolysis and ozone, *J. Geophys. Res.*, *110*, D23206, doi:10.1029/2005JD005898.

Li, G., R. Zhang, J. Fan, and X. Tie (2007), Impacts of biogenic emissions on photochemical ozone production in Houston, Texas, *J. Geophys. Res.*, *112*, D10309, doi:10.1029/2006JD007924.

Liu, G., H. Shao, J. A. Coakley Jr., J. A. Curry, J. A. Haggerty, and M. A. Tschudi (2003), Retrieval of cloud droplet size from visible and microwave radiometric measurements during INDOEX, *J. Geophys. Res.*, *108*(D1), 4006, doi:10.1029/2001JD001395.

Lynn, B. H., A. P. Khain, J. Dudhia, D. Rosenfeld, A. Pokrovsky, and A. Seifert (2005a), Spectral (Bin) microphysics coupled with a mesoscale model (MM5). Part I: model description and first results, *Monthly Weather Review*, *133*, 44–58.

Lynn, B. H., A. P. Khain, J. Dudhia, D. Rosenfeld, A. Pokrovsky, and A. Seifert (2005b), Spectral (Bin) microphysics coupled with a mesoscale model (MM5). Part II: simulation of a CaPE rain event with a squall line, *Monthly Weather Review*, *133*, 59–71.

Maritinsson, B. C., et al. (1999), Droplet nucleation and growth in orographic clouds in relation to the aerosol population, *Atmos. Res.*, *50*, 289–315.

Meyers, M. P., P. J. DeMott, and W. R. Cotton (1992), New primary ice-nucleation parameterizations in an explicit cloud model, *J. Appl. Meteor.*, *31*, 708–721.

Nesbitt, S. W., R. Zhang, and R. E. Orville (2000), Seasonal and global NOx production by lightning estimated from the Optical Transient Detector (OTD), *Tellus B*, *52*, 1206–1215.

Ohashi, Y., and H. Kida (2002), Local circulations developed in the vicinity of both coastal and inland urban areas: a numerical study with a mesoscale atmospheric model, *J. of Appl. Meteorl.*, *41*, 30–45.

Orville, R. E., G. Huffines, J. Nielsen-Gammon, R. Zhang, B. Ely, S. Steiger, S. Phillips, S. Allen, and W. Read (2001), Enhancement of cloud-to-ground lightning over Houston, Texas, *Geophys. Res. Lett.*, *28*, 2597–2600.

Penner, J. E., et al. (2001) Aerosols, their direct and indirect effects, in *Climate Change 2001: The Scientific Basis,* edited by J. T. Houghton et al., Cambridge Univ. Press, New York, 289–348.

Ramanathan, V., et al. (2001), The Indian Experiment: An integrated assessment of the climate forcing and the effects of the great indo-asian haze, *J. Geophys. Res.*, *106*, 28,371–28,398.

Ramaswamy, V., et al. (2001), Radiative forcing of climate change, in *Climate Change 2001: The Scientific Basis*, edited by J. T. Houghton et al., Cambridge Univ. Press, New York, pp. 349–416.

Reisin, T., Z. Levin, and S. Tzvion (1996), Rain production in convective clouds as simulated in an axisymmetric model with detailed microphysics. Part II: Effects of varying drops and ice initiation, *J. Atmos. Sci.*, *53*, 1815–1837.

Rosenfeld, D. (2000), Suppression of rain and snow by urban and industrial air pollution, *Science*, *287*, 1793–1796.

Rosenfeld, D., and W. Woodley (2001), Pollution and Clouds, *Physics World*, 33–37.

Shepherd, J. M., and S. J. Burian (2003), Detection of urban-induced rainfall anomalies in a major coastal city, *Earth Interactions*, *7*, doi:10.1175/1087-3562.

Twomey, S. (1977), The influence of pollution on the shortwave albedo of clouds, *J. Atmos. Sci.*, *34*, 1149–1152.

Wang, C. (2005), A modeling study of the response of tropical deep convection to the increase of cloud condensation nuclei concentration: 1. Dynamics and microphysics, *J. Geophys. Res.*, *110*, D21211, doi:10.1029/2004JD005720.

Williams, E. R., R. Zhang, and J. Rydock (1991), Mixed phase microphysics and cloud electrification, *J. Atmos. Sci.*, *48*, 2195–2203.

Xue, H., and G. Feingold (2006), Large-eddy simulations of trade wind cumuli: Investigation of aerosol indirect effects, *J. Atmos. Sci.*, *63*, 1605–1622.

Yin, Y., Z. Levin, T. Reisin, and S. Tzivion (2000), Seeding convective clouds with hygroscopic flares: Numerical simulations using a cloud model with detailed microphysics, *J. Appl. Meteor.*, *39*, 1460–1472.

Zhang, R., X. Tie, and D. W. Bond (2003), Impacts of anthropogenic and natural $NO_x$ sources over the U. S. on tropospheric chemistry, *Proc. Natl. Acad. Sci. U. S. A.*, *100*, 1505–1509.

Zhang, R., I. Suh, J. Zhao, D. Zhang, E. C. Fortner, X. Tie, L. T. Molina, and M. J. Molina (2004a), Atmospheric new particle formation enhanced by organic acids, *Science*, *304*, 1487–1490.

Zhang, R., W. Lei, X. Tie, and P. Hess (2004b), Industrial emissions cause extreme diurnal urban ozone variability, *Proc. Natl. Acad. Sci. USA*, *101*, 6346–6350.

Zhang, R., G. Li, J. Fan, D. L. Wu, E. R. Williams, and M. J. Molina (2007), Intensification of Pacific storm track linked to Asian pollution, *Proc. Natl. Acad. Sci. USA*, *104*, 5295–5299.

J. Fan, G. Li, and R. Zhang, Department of Atmospheric Sciences, Texas A&M University, College Station, TX 77843, USA. (zhang@ariel.met.tamu.edu)

W.-K. Tao, NASA Goddard Space Flight Center, Code 613.1, Greenbelt, MD 20771, USA.